







# Using structural colour to track length scale of cell-wall layers in developing *Pollia japonica* fruits

Rox Middleton<sup>1,2</sup> , Edwige Moyroud<sup>3</sup> , Paula J. Rudall<sup>4</sup> , Christina J. Prychid<sup>4</sup> , Maria Conejero<sup>4</sup> ,  
Beverley J. Glover<sup>5</sup>  and Silvia Vignolini<sup>1</sup> 

<sup>1</sup>Chemistry Department, University of Cambridge, Cambridge, CB2 1EW, UK; <sup>2</sup>Department of Life Sciences, University of Bristol, Bristol, BS8 1TQ, UK; <sup>3</sup>Sainsbury Laboratory, University of Cambridge, Cambridge, CB2 1LR, UK; <sup>4</sup>Royal Botanic Gardens Kew, Richmond, Surrey, TW9 3AB, UK; <sup>5</sup>Department of Plant Sciences, University of Cambridge, Cambridge, CB2 3EA, UK

## Summary

Authors for correspondence:  
Rox Middleton  
Email: rmm.middleton@gmail.com

Beverley J. Glover  
Email: bjg26@cam.ac.uk

Silvia Vignolini  
Email: sv319@cam.ac.uk

Received: 1 December 2020  
Accepted: 5 March 2021

New Phytologist (2021)  
doi: 10.1111/nph.17346

**Key words:** biomaterials, cell wall, cell-wall development, helicoidal cellulose, morphogenesis, nanostructure, structural colour.

- Helicoidally arranged layers of cellulose microfibrils in plant cell walls can produce strong and vivid coloration in a wide range of species. Despite its significance, the morphogenesis of cell walls, whether reflective or not, is not fully understood. Here we show that by optically monitoring the reflectance of *Pollia japonica* fruits during development we can directly map structural changes of the cell wall on a scale of tens of nanometres.
- Visible-light reflectance spectra from individual living cells were measured throughout the fruit maturation process and compared with numerical models.
- Our analysis reveals that periodic spacing of the helicoidal architecture remains unchanged throughout fruit development, suggesting that interactions in the cell-wall polysaccharides lead to a fixed twisting angle of cellulose helicoids in the cell wall.
- By contrast with conventional electron microscopy, which requires analysis of different fixed specimens at different stages of development, the noninvasive optical technique we present allowed us to directly monitor live structural changes in biological photonic systems as they develop. This method therefore is applicable to investigations of photonic tissues in other organisms.

## Introduction

Both plants and animals can produce structural colouration by exploiting layered structures at the submicron-scale consisting of materials with different refractive indices (Kinoshita & Yoshioka, 2005). This widespread strategy requires exquisite optimization of the layer size and spacing of the materials to generate the diversity of colours and optical effects recorded in the natural world (McDonald *et al.*, 2017). In some plants, similar layered structures can be produced by cell-wall assembly of cellulose fibrils in an helicoidal architecture (Middleton *et al.*, 2016). Such architectures have been observed in various organs of several distantly related plant species, including the leaves of the monocot *Mapania caudata* (Strout *et al.*, 2013) and the fern *Microsorium thailandicum* (Steiner *et al.*, 2018), the fruits of the eudicot *Margaritaria nobilis* (Vignolini *et al.*, 2016) and the monocot *Pollia condensata* (Vignolini, Rudall, *et al.*, 2012). In this architecture, microfibrils are organized parallel to each other in quasi-planes, where adjacent planes are rotated at a slight angle with respect to one

another, producing a chiral structure. The intrinsic birefringence of the microfibrils (i.e. different refractive index along and perpendicular to the fibril direction) gives the helicoid structure a periodically changing refractive index which, when its repeated dimension (called “pitch”) is resonant with visible wavelengths, produces a brightly coloured reflection.

Interestingly, similar helicoid architectures at nonoptical scales also have been reported in algae (Neville & Levy, 1984) and animals (Belamie *et al.*, 2006), and particularly prominently in crustaceans (Chen *et al.*, 2008). In many materials, these helicoidal ‘plywoods’ function as a toughening strategy (Giraud-Guille, 1998). They also are found in insects (Bouligand, 1972), although optical-wavelength scale helicoids also are very common in insect exocuticle. In animal biomaterials, helicoids are composed of collagen or chitin rather than cellulosic molecules. Despite the abundance of such helicoidal architectures in both plants and insects (Sharma *et al.*, 2009), very little research has been undertaken on the mechanisms underpinning their development and the biological processes leading to their formation remain largely unknown.

Understanding the mechanisms controlling microfibril architecture as helicoids develop within living tissues remains an open and important challenge that applies to the understanding of plant cell walls in general, including those not producing structural colour. To date, research on the development of helicoidal cellulose architectures has been limited to the pioneering work of Reis (Reis *et al.*, 1991, 1994; Roland *et al.*, 1987) and Neville and co-workers (Neville, 1985).

In this study, we observed the maturation of *Pollia japonica* fruits (Fig. 1a–d), the cell walls of which are composed of optically reflective helicoidal cellulose. We used optical techniques and numerical modelling to perform a real-time analysis that is noninvasive and nondestructive to measure structural changes in living cell walls at a scale of tens of nanometres.

Developmental imaging of internal and nanometric structures is challenging in complex living organisms, as many high-precision anatomical techniques require destructive imaging, necessarily implying that the same material cannot be repeatedly imaged through development. Other noninvasive techniques such as nanoCT theoretically have a minimum resolution of 50 nm, although in practice currently *c.* 120 nm (Sykes *et al.*, 2019); they also lack capacity to image structure within dense continuous materials.

In this study, we used an optical model (based on 4 × 4 Matrix technique; Berreman, 1972) developed for light propagation in

liquid crystals (Oseen, 1932) that treats the reflective cell wall as a chiral nematic structure, as in a cholesteric liquid. ‘Chiral nematic’ refers to the same helicoidal ‘plywood’ geometry in a liquid crystal. As the intensity and peak wavelength reflected by these helicoidal architectures is strongly sensitive to their morphological parameters, in particular to the pitch length and number of repeated pitches, we can observe real-time nanometric changes in the developing cell wall.

Cell-wall development proceeds by the layering of fibres from the internal cell, producing the outer surface first. How exactly the cell wall is built remains unconfirmed. Structural changes in the cell wall are predicted by different mechanisms that might explain this development. For example, Neville’s liquid crystal hypothesis (Neville & Levy, 1984) proposed that compaction might be a necessary feature of cell-wall development, as it is in cellulose nanocrystal self-assembly (R. M. Parker *et al.*, 2017). Therefore, investigating the cell-wall morphological dynamics during development is crucial to understanding how cell walls are laid down in general.

Finally, to evaluate the effectiveness of our method, we compare it with the most common and highest resolution technique for internal structural imaging, transmission electron microscopy (TEM), which has been used successfully on a wide range of biological samples, from beetle elytra (A. R. Parker *et al.*, 1998) to leaf iridoplasts (Jacobs *et al.*, 2016; Onelli *et al.*, 2017).

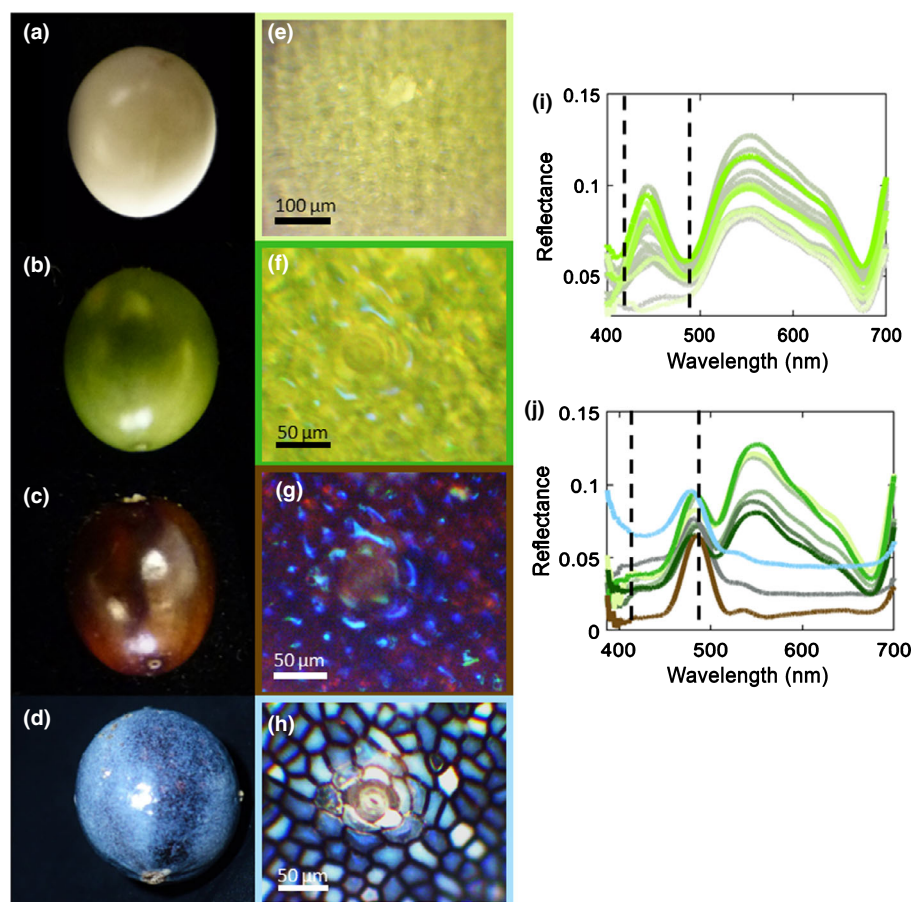


**Fig. 1** Developmental stages of *Pollia japonica* fruits. (a–d) Macroscale images of *P. japonica* fruits at four characteristic stages of the ripening process (from day (D)1 to *c.* D33), top to bottom chronologically. (e–h) Corresponding optical microscopy images of epidermal cells at different maturation stages, obtained using crossed-polarizers to remove surface glare. Cells were chosen adjacent to a stomatal pore to ensure reproducible location. (i) Spectra recorded over the first 5 d from the central reflection for one cell normalized with respect to an aluminium mirror. (j) Spectra recorded from the central reflection of a different cell through the final three stages of maturation (green, brown and blue stages) from D7 to D24. Intensity given with respect to perfect reflection of left circularly polarised light. Vertical dashed lines indicate range of structural colour peak. In both (i) and (j) only every tenth spectrum is shown for clarity. Full data series are shown in Supporting Information Fig. S1(c) (for (i)) and Fig. S2 (for (j)). Line colours indicate approximate overall fruit colour at this chronological point, colour transition moves from white – light green – dark green – brown – blue and correspond to the borders of (e–h).

## Materials and Methods

### Living fruit specimens

Cells were measured directly from fruits maturing on (*c.* 50-cm-tall) living *Pollia japonica* plants that had been grown from seed (B&T World Seeds, Pagnignan, Aigues-Vives, France) for 2 yr in Levington's (UK) M3 compost. Plants were grown at variable humidity in the University of Cambridge Department of Plant Sciences greenhouse at  $23 \pm 3^\circ\text{C}$  and received supplemental lighting from Osram 400 W high-pressure sodium lamps (Osram, Munich, Germany) on a 16 h : 8 h, light : dark photoperiod.

Compared with structurally coloured fruits of *Pollia condensata*, the fruits of *P. japonica* are relatively easy to manipulate: the surface of the fruit (epicarp) is directly exposed during growth rather than covered by a perianth, fruits are separated from each other due to an expanded inflorescence, and the fruit maturation time is relatively short (*c.* 1 month).

### Optical microscopy

Optical imaging using light microscopy (LM) was performed using a customized Zeiss (AxioScope A.1) optical microscope equipped with a polarizer and a super-achromatic quarter waveplate (Bernhard Halle Nachfl. GmbH, Berlin, Germany) mounted onto independent motorized rotation stages in the optical path to perform polarization-resolved imaging. A manual rotation linear polarization filter (Thorlabs 427710-9000; Thorlabs Inc., Newton, NJ, USA) was additionally used for illumination. The two polarizers were used for crossed-polarization imaging and spectroscopy. Imaging was done using cross-polarized light in order to cut all the surface reflection, therefore better identifying the reflectance spot. Measurements were taken using left-handed polarized light in order to maximize collected light. The quarter waveplate was used in conjunction with the second filter for calibration references. The reflection microscopy body was in standard Koehler illumination configuration using a standard halogen lamp. Koehler illumination places the image and lamp in inverse focal planes, thus avoiding image overlap. This reflectance microscope was mounted on a tower with a specimen clearance of  $\leq 38$  cm, which allowed for the entire plant to be in place under the objective, the stem slightly bent and fixed near the top to an upright metal rod on an *x-y* manual screw-stage which allowed for the minute lateral movement of the fruit in the focal plane of the objective.

For imaging and spectrometry, a Long-Distance EC Epiplan Neofluar  $\times 20/0.22$  objective lens (Zeiss) was used in Bright Field configuration with a small ( $\pm 5^\circ$ ) numerical aperture of illumination introduced by a Fourier plane numerical aperture. Low numerical aperture is important in order to collect on-axis reflected light. Images were captured by a CCD camera (DCC3240C (Thorlabs) or IDS UI-3580LE-C-HQ (Imaging Development Systems, Obersulm, Germany)), accessed via THORCAM/UEYE COCKPIT user interface software. Visible-light reflectance spectra were taken alongside photographs from the central point in a confocal

30  $\mu\text{m}$  spot coupled into an optical fibre (50  $\mu\text{m}$  core diameter; Avantes, Apeldoorn, the Netherlands) and measured using a visible-range spectrometer (Avaspec-HS2048; Avantes). Reflectance spectra were normalized with respect to an aluminium mirror (PF10-03-P01 25.4 mm; Thorlabs).

### Cell identification

In order to perform the spectroscopic analysis of a single cell, it is important to clearly and repeatably define its location. The position of the cell therefore was identified by the cell contour and by its orientation with respect to other cells and surface features, for example the stomatal pore visible in Fig. 1.

The cell contour is visible using a parallel polarization to accentuate the surface contours. A set of cells were identified under the microscope using multiple polarization filters to identify cell-wall boundaries and mapped for re-identification, as shown in Fig. S3. Measurements were taken from the centre of each cell, where a coloured spot developed during maturation. It is the optical reflectance spectrum of this coloured spot that is characterized in order to model the helicoidal photonic material. For each identified cell, a set of visible-light spectra was recorded at each measurement time point.

Initially, 29 individual cells were measured at regular intervals throughout the day on a single fruit. Measurement times were decreased from an initial hourly frequency to once every 4 h over the first 5 d of maturation through the white to green stage transition.

Subsequently, a second set of 23 cells on a different fruit of the same plant, at approximately the same stage of development, was measured in a similar way but with a reduced frequency of up to only twice a day for 17 d over the remaining ripening period (green-blue stages), until they reached a stable visually mature appearance.

### Spectral processing

Spectral measurements were taken from the centre of the cell, where the bright structural colour spot develops. Nevertheless, each measurement collects light of both pigmentary and structural origin. In order to understand the change in structural colour, the spectra were processed to remove the effect of pigmentation by subtracting an intensity-scaled, synchronous but purely pigmentary spectrum from a location where structural colour did not develop. An example of this processing is shown graphically in Supporting Information Fig. S1. Structural colour peaks were characterized by peak wavelength and intensity of the narrow single peaked structural colour reflectance spectrum and using a fitted Gaussian peak. A linear mixed-effects model was applied to the peak characteristics over the maturation period to reveal overall trends in the cells.

### Electron microscopy

Electron microscopy techniques were used to investigate the anatomy of the epidermis and the internal structure of

structurally coloured cells, using both resin-embedded microtomed samples and nonembedded fresh samples.

For scanning electron microscopy (SEM), nonembedded fruit material was fractured and mounted on an aluminium stub with carbon tape. Samples were sputter-coated with 10nm Pt (Q150T ES Turbo-Pumped Sputter Coater; Quorum Technologies Ltd, Lewes, UK) and observed using a Zeiss Leo Gemini 1530VP SEM at between 3 and 5 kV.

For transmission electron microscopy (TEM), fruits were cut into small fragments and fixed in 3% phosphate-buffered glutaraldehyde followed by 1% osmium tetroxide. Fixed samples were taken through a graded ethanol and LR White resin series before embedding. Ultrathin sections (50–100 nm) were cut using an ultramicrotome (Reichert-Jung Ultracut; Leica Biosystems, Nussloch, Germany), collected on formvar-coated copper slot grids, and post-stained with uranyl acetate and lead citrate. Samples were imaged using a H-7650 TEM (Hitachi, Tokyo, Japan) with integral AMT XR41 digital camera. Some of the resin-embedded blocks subsequently were imaged on the SEM after sectioning.

### Numerical model

A numerical model implementing the Berreman  $4 \times 4$  matrix technique (Berreman, 1972) for a helicoid composed of cellulose with refractive index of  $n_c/n_o = 1.586/1.524$  (Dumanli *et al.*, 2014; Steiner *et al.*, 2018) was used to compute the visible-light reflectance spectrum for the pitch profiles extracted from the TEM images. Upper and lower refractive index boundaries were  $n_{\text{above}} = 1.33$ , representing water, and  $n_{\text{below}} = 1.55$ , representing organic material –predominantly cellulosic – in order to remove the effect of the outer surface reflectance, which in spectrometry was done by using cross-polarized light. The effect of variation of the disorder in the pitch profile was introduced by considering a normally distributed pitch profile ( $\mu = 149$  nm,  $\sigma = 19$  nm). This distribution may be chosen by measurement from electron microscopy cross-sections, or else selected to produce a peak with peak wavelength corresponding to experimental measurement. Angle of incidence was modelled as normal ( $0^\circ$ ), in order to replicate the conditions of the experimental measurements in which the numerical aperture of incident light was constrained to  $\pm 5^\circ$  by an additional source-plane numerical aperture and reflected light collected from angles close to the optical axis. This variation produced a negligible difference in modelled visible-light spectra. The effect of cell curvature and off-normal refraction is ignored owing to the difficulty in introducing accurate proportions of curvature, and the low degree of curvature in EM images of upper cell walls at all developmental stages, see Fig. S4.

The final intensity of the model was reduced to 20% to account for loss from random scattering, absorption or other imperfection, rather than attempting to define each of these factors separately in the model. However, this scaling value was chosen to match the characteristic intensity of the fully developed cell-wall model to the fully developed cell reflectance measurement, and thus should not be taken as predictive. It should be noted that the model is consistently scaled at all stages of development.

## Results

### Stages of development in *Pollia japonica* fruits

In our growth conditions, the development of mature *P. japonica* fruits takes about a month and four characteristic stages (shown in Fig. 1a–d) can be identified based on the visual appearance of the fruits. Stages of maturity of the fruit can be characterized as white, green, brown and blue (fully mature).

The montage in Fig. 2(a) shows that each cell undergoes clear individual transitions. The majority (12–16 d) of the development period is spent in the green phase, with the brown phase lasting just 3–5 d. Once mature, the matte variegated light and dark blue appearance remains stable over several decades, as observed by comparison of newly developed fruits with dried samples from 1986 (Bartholemew *et al.*, 1986). The fruits do not significantly change shape or size during the maturation period described, but at maturity they become dry and consist of a brittle epidermal layer enclosing loose seeds. The mature, indehiscent (i.e. not splitting when ripe) fruits remain intact and firmly attached to long pedicels, even after the stems have dried completely.

The transition between the first two developmental stages is relatively difficult to define, with the white phase lasting for about a week as the green appearance due to formation of chlorophyll becomes more pronounced (see Fig. 1). Cells appear a mottled very pale green colour (Fig. 1e) which gradually brightens to a deep green very characteristic of chlorophyll pigmentary scattering, both in colour and the shape of the optical reflectance spectrum.

As the cell matures into the green stage a (blue) reflectance spot develops in the centre of the cell, this can be seen in the images and spectra in Fig. 1(b–d, f–h). An overview of isolated cell images as each develops is shown in the montage in Fig. 2(a). This pattern of reflectance is caused by the cell curvature and previously has been explained by work on the closely related plant *P. condensata* (Vignolini *et al.*, 2012). Unlike in *P. condensata*, the reflective cells in *P. japonica* are found only in a single outer layer, above layers of thin-walled pigmented cells, as shown in the SEM and schematic in Fig. 2(b,c). As a consequence of this single layer, the reflectance spot for each cell may be unambiguously identified and is evident in each element of the montage in Fig. 2(a).

By contrast with the gradual change from white to green phases, the two subsequent developmental transitions are more defined. The green of active chlorophyll in each cell no longer dominates and a brownish colour pigment is observed. This makes the bright blue spots more obvious, and cells appear clearly distinct from one another (Fig. 1g). Finally, a sudden dehydration produces a bright blue-ish broadband scattering reflectance from the entire cell body, although the blue spot is still clear. In this final stage, the cell walls stand out as dark borders between each brightly reflecting cell body (Fig. 1h).

The change from green to brown correlates to the loss of the characteristic chlorophyll signature in the reflectance spectra, as a dark brown pigment dominates the cell contents. However, the

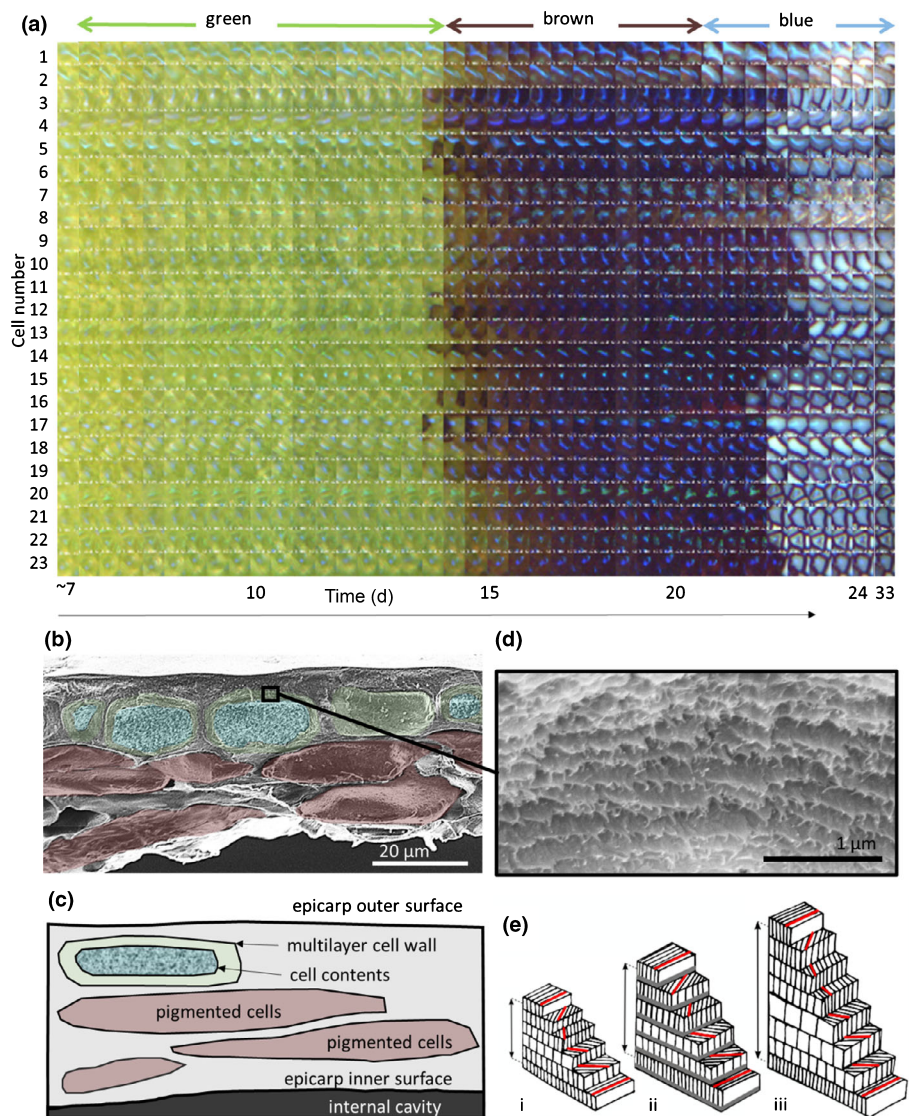


**Fig. 2** The optical signal from the photonic nanostructure becomes dominant over chlorophyll pigmentation during *Pollia japonica* fruit maturation. (a) Repeated images of each of 23 observed epidermal cells over the second maturation period (> 7 d), transitioning from green, to brown through to blue stages. Each stage is precisely labelled for cell #1 although other cells transition at slightly different times. The column furthest on the right shows the same cells 9 d after daily measurement ended. The second recorded time-set of images is not shown because of a miscalibrated white balance on the camera that did not affect the spectral measurement. (b) False-colour scanning electron microscopy (SEM) cross-section through the mature epicarp of *P. japonica* fruits. The colour used corresponds to that in (c), a labelled schematic depicting different parts of the epicarp tissue in (b). (d) Higher magnification SEM showing internal structure of cell wall. (e) Schematic showing three helicoidal stacks of different pitch lengths, indicated by the arrows. Longer pitches are produced by increased layer thickness (i vs ii) or decreased angular offset (i vs iii).

component of structural colour, which produces significant blue reflectance which comes to dominate the appearance of the fruit is present during the stage where chlorophyll scattering dominates. Structural colour is reflected from the cell walls of the outer cells, as shown in the schematic of Fig. 2(c), and the higher magnification SEM image in Fig. 2(d). This image shows the cellulosic layers of the cell wall, which are arranged in a helicoidal architecture, as schematized in Fig. 2(e). It is this architecture that analysis of the structural colour reflectance spectrum investigates, because the nanometric lengthscale of the structure – the pitch indicated by arrows – determines the spectrum characteristics; the peak wavelength corresponds to twice the pitch length. An increase in pitch length may be the result of a change in the width of each effective layer, or the offset angle between each layer.

The transition from brown/black with a central blue spot, to a bright whitish-blue can occur suddenly (see Fig. 3a–c). The cells change from a single blue reflectance point within a dark pigmented cell, to a bright reflective cell, with a blue reflection spot still visible. The transition is caused by dehydration of the cell

and may be visually reversed by the application of water, shown in Fig. 3. The dehydration transition produces an additional broadband scattering from the granular contents inside the cell (visible in Fig. 2b and at higher magnification in Fig. S4h). This combines with blue reflectance from the helicoidal multilayer. This scattering is not from coloured pigments, as in the earlier stages, but occurs as dehydration produces interfaces of high refractive index contrast within the porous cell contents. Reflection from refractive index interfaces in granular structures is a common cause of broadband scattering, as in foam. This transition occurs naturally on the plant. Under the heat of the microscope illumination the process occurs over a fraction of a second; this also may be the case in vivo.

### Spectral characteristics of individual epidermal cells during fruit maturation in *P. japonica*

Of the first group of monitored cells, 21 developed a coloured spot from the centre during the observation period and were

included in the analysis. The reflectance data of another eight cells were discarded as either they were not recorded at each time-point, or they were acquired from locations that did not develop any colour, for example the nonreflective edge region of a large cell. Of the second group of monitored cells, bright reflection spots were visible in all.

Figure 4 shows plots of the peak intensity of the first period and peak wavelength over the two periods of maturation separately (first 5 d of maturation (white stage) and >7 d of maturation (green to blue stage)). Owing to the lack of a control cell in the second period, as all measurement points formed a structural colour reflectance spot, the intensity of structural colour peak could not be extracted from the overall spectra, although the peak wavelength remained possible to extract.

Transitions in intensity and peak wavelength were plotted for each cell and are shown in Fig. 4. Individual cells showed an increase in intensity over the first period of maturation (Fig. 4a), but no change in peak wavelength during either maturation period (Fig. 4b,c).

A linear mixed effects model was used in order to understand the temporal transition of the cohort of cells in intensity and wavelength independent of the variation between cells. The linear mixed effects fit and 95% confidence intervals (CI) are plotted on each graph in Fig. 4.

As expected, the intensity of the reflectance is observed to increase over the initial maturation phase. The fit shows an average increase in the reflectance intensity of  $1.3 \pm 0.4\%$  of light incident over 5 d, and close to doubling the total reflectance intensity of the structural colour. This transition is independent of the change in intensity resulting from pigment scattering, and any reflectance from the glossy outer surface, as both factors have been removed. The intensity of the structural colour therefore is clearly observed to increase during the early stage of maturation.

## Optical model

We developed an optical model, as detailed in the methods section, to explain the observed spectral measurements. The optical model is shown in Fig. 5(a) alongside experimental data in panel (a). The optical model reproduces the helicoidal anisotropic architecture with a normally distributed set of pitches to reproduce the variation observed in the natural material. It is this variation that allows a cholesteric model to reproduce the broadened waveband peak.

Minimal numbers of layers were used in order to reproduce the earliest stages of wall thickening, while also generating a defined colour peak. The numbers of repeated pitches used in our optical model were later validated by cross-checking with the number of layers observed in TEM cross-sections (see Fig. 6). Although the spacing could be affected by TEM artefacts (King, 1991), the number of identifiable layers is not.

As expected, an increase in the number of layers of the cell wall closely models the increase in the reflectance intensity that is observed in the trends across all the measured cells. This observation corresponds with an increase in the thickness of the reflecting cell wall during this time. The first maturation phase is therefore confirmed as a period of active cell-wall thickening.

As seen in the experimental data in Figs 4(b,c), 5(b), the peak wavelength position does not change during the initial growth period. We therefore used the model to fit the periodic pitch of the helicoid. From the optical model we observe that the value of the pitch length can be measured with very high accuracy on a single cell. In fact, the changes recorded during the observation periods are far smaller (first period +0.5 nm, second period -1.5 nm) than the resolution of experimental error (95% CI for linear fit on each cell =  $\pm 8.4$  nm, see Fig. S5). We conclude that the pitch of the helicoidal cell wall is fixed during maturation.

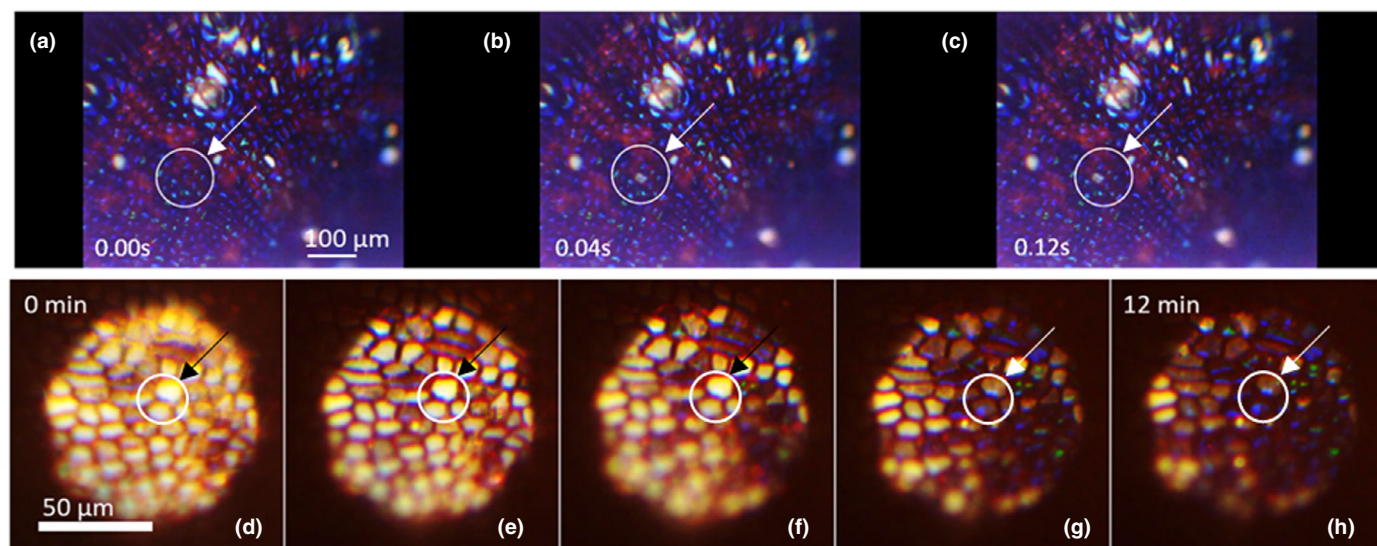


**Fig. 3** Dehydration and rehydration of *Pollia japonica* fruits. (a–c) Rapid dehydration during last stage of fruit maturation from brown (at 0.0 s) to blue (at 0.04 s and 0.12 s) stages. Imaged dry with cross-polarizers. One cell in the centre of the circled area undergoes dehydration during these frames. (d–h) Frames from a video of one area during artificial rehydration by application of water using a water-immersion objective lens. Water infiltration reduces scattering within each cell, allowing the clear appearance of the bright reflectance spot again. A circle shows the same two cells in each frame as they rehydrate.

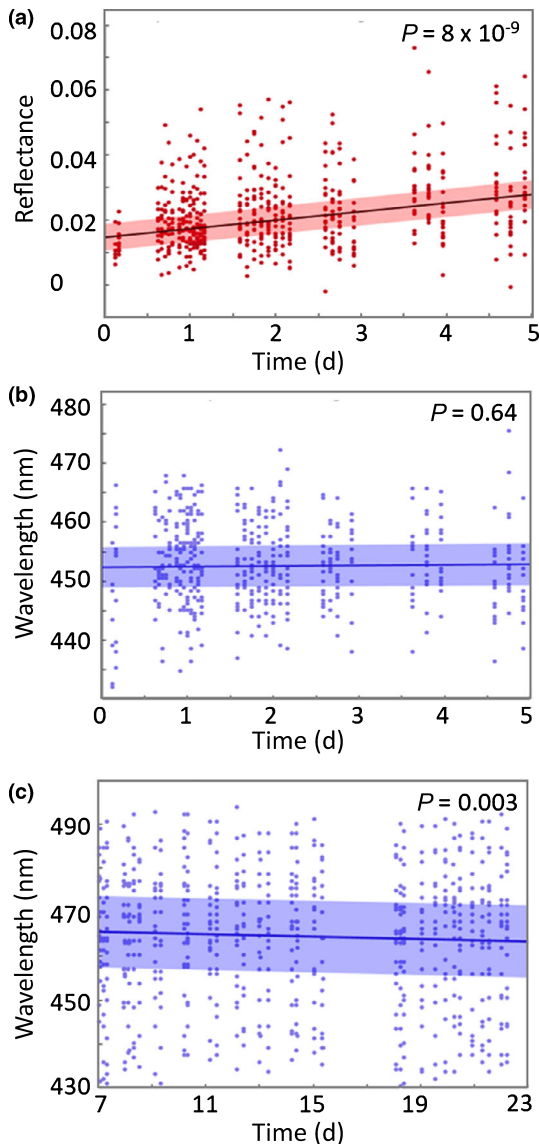


**Fig. 4** Statistical analysis of wavelength trends during *Pollia japonica* fruit maturation. (a) Reflectance intensity of full set of cells over first 5 d (white stage, first period of maturation) and linear mixed effects fit and  $\pm 95\%$  confidence intervals, normalized with respect to a mirror. (b) Corresponding peak wavelength of all cells over first 5 d (white stage, first period of maturation). (c) Wavelength change over the second maturation period ( $> 7$  d, from green stage to blue stage).

### TEM analysis of cell-wall structure change between immature and mature stages

In order to compare the cell wall anatomy inferred from the experimental spectra and the model, transverse sections of fruits at different stages of development were imaged in TEM, shown in Fig. 6(a–c). In the samples measured, cell walls of fully mature fruits (blue stage) had increased numbers of layers compared with immature white stage fruits, as predicted by the optical model. However, the cell-wall pitches were longer in white stage fruits.

Anatomical parameters of the cell wall (number of layers and periodicity) were extracted from the TEM images and used in the optical model to understand what colour would be reflected,

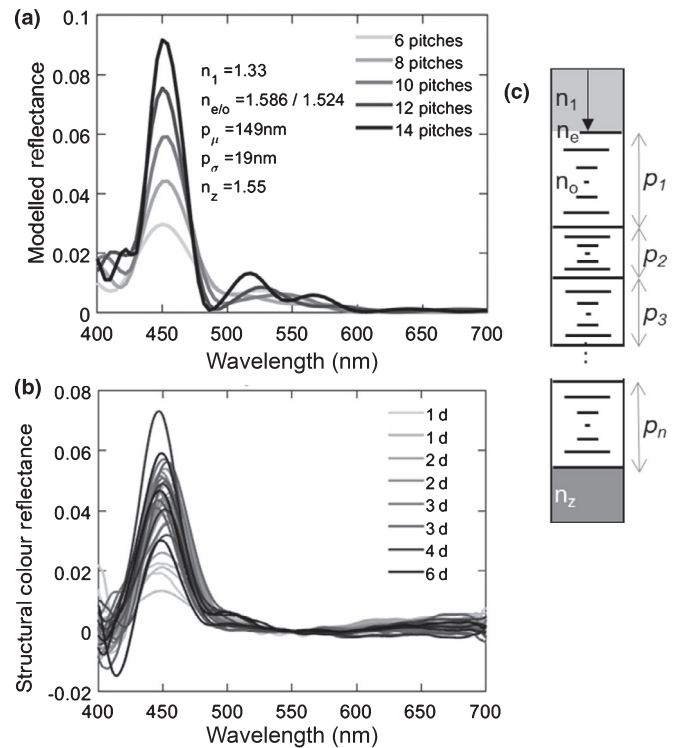


**Fig. 5** Modelling the visible spectral change at the cellular level during the first maturation period of *Pollia japonica* fruits. (a) Numerically modelled profile of a cellulose helicoidal multilayer with mean averaged over five statistically distributed profiles. (b) Change in structurally coloured peak in one cell over first 5 d of measurement (white stage). The pigmented, chlorophyll-derived component has been removed using an intensity-normalized control spectral series. Intensity normalized with respect to an aluminium mirror. (c) Schematic showing the numerical model parameters for model shown in (a).  $p_{1...n}$  are distributed normally according to parameters shown in (a), where  $p_{\mu}$  is the average pitch, modelled to be 149 nm,  $p_{\sigma}$  is the SD of the pitch, and  $n$  is the refractive index of the material.  $n_{e/o}$  refers to the two refractive indices of the anisotropic helicoidal material.

assuming no change in dimensions during preparation for TEM. The anisotropic refractive indices ( $n_{e/o}$ ) were varied within reasonable ranges, as the influence of expansion on effective refractive index is unknown. The corresponding spectra are shown in Fig. 6(d–f). As expected, the predicted reflectance spectra in the earlier stages peak far outside of the range of observed cell reflectances at any stage (shown in blue shaded box).

Even accounting for a change in refractive index, these results therefore would suggest that at later stages of fruit development, the cellulose fibres undergo an overall compression of the helicoidal structure and thus a change in peak reflected wavelength of several hundred nanometres, by contrast with our experimental observations.

### Discussion

Although transmission electron microscopy (TEM) is a widely accepted conventional approach to study cell-wall anatomy, important limitations exist when it comes to the quantitative assessment of nanometric structures in biomaterials. Indeed,

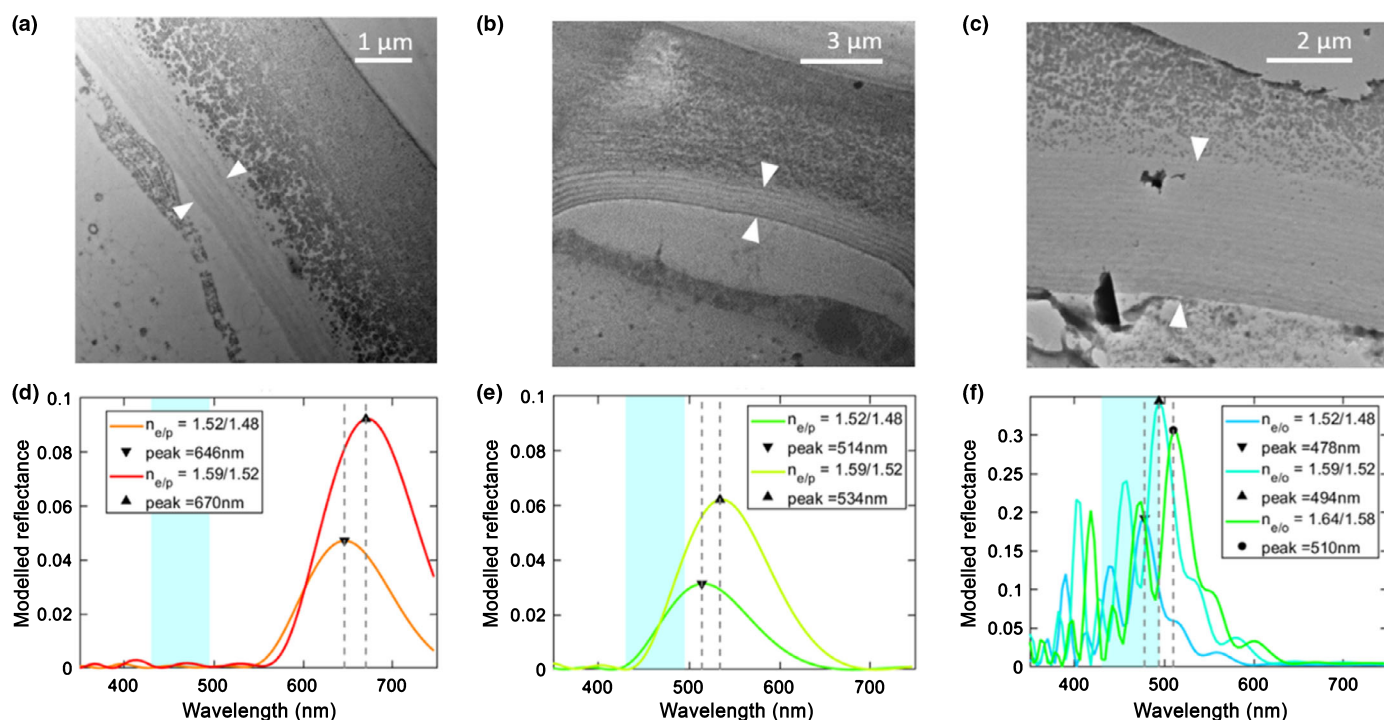


**Fig. 6** Transmission electron microscopy (TEM) cross-section images of *Pollia japonica* cells used to extract cell-wall parameters to inform optical modelling (a,b), TEM image of a cross-section through helicoidal outer cell walls at immature white stage. (c) TEM image of a cross-section through the outer cell wall at blue mature stage (d–f). Plots of modelled reflectance peak from each corresponding TEM (image above). Two sets of refractive indices were compared:  $n_{e/o} = 1.586/1.524$  (Dumanli *et al.*, 2014; Steiner *et al.*, 2018) and a lowest reasonable bound (dashed line)  $n_{e/o} = 1.519/1.477$  (taken from other low refractive index, higher liquid content materials like lipids) and in (f) an additional, upper bounded set of values are shown  $n_{e/o} = 1.64/1.58$ . This was in order to ensure that refractive index changes caused by changed in composition might not counteract a change in pitch length as measured by TEM. Still, this would predict a change in reflected wavelength during maturation. The range of experimentally measured peak reflectance wavelengths is indicated in blue shading. The reflectance intensity is not scaled to 20% as in the model in Fig. 5 and is thus considered as an ideal case, free from defects and scattering elements.

the fixation and embedding process preceding TEM imaging is known to introduce significant changes in structure dimensions: for example, resin-embedding and microtome sectioning produce differential artefacts, the magnitude and characteristics of which depend on the specific tissue and conditions (King, 1991). In the case of *Pollia japonica* fruits, we expect that cell walls at different stages of development have different characteristics (such as water content), resulting in variable swelling or contraction in fixative.

Moreover, TEM investigation is not compatible with live imaging and cell-tracking over any period of time. To investigate a developmental series using TEM necessarily requires samples to be taken from separate fruits at each maturation stage, and therefore analyzes different cells. As there is a range of final peak wavelengths observed in mature cells, observable developmental change could be confounded by natural intercell variation, even if embedding artefacts could be suppressed.

Combining spectroscopy with an optical model for the cell wall, we show here that it is possible to overcome these issues and monitor cell-wall development noninvasively and with increased accuracy. We observed that structural colour appears in the fruits of *P. japonica* at very early stages, even before it contributes to the overall visual appearance of the fruit which initially is dominated by pigments. This finding is consistent with observations using electron microscopy of helicoidal layers in early stage fruits. The

ability to measure the reflectance from even these very few layers confirms the suitability of the optical model for the system.

By measuring the same individual cells throughout the maturation process of living fruits *in situ* on *P. japonica* plants, our new approach also establishes a high degree of stability in the characteristic length scales of the repeated helicoidal pitches within the cell wall during the entire maturation. This observation contrasts with results of the TEM analysis, which indicates a change in the characteristic length scales during growth. We have shown that, when artefacts induced by tissue fixation and processing required for conventional electron microscopy technique are avoided, thickening cell walls have no lateral expansion or compression in this species.

Interpreting this result in order to understand cell-wall development suggests a gradual accretion of cell-wall material in its permanent configuration without compaction, allowing for cell-wall internal rearrangement other than by lateral movement. This observation therefore supports the hypothesis of growth proposed by Reis *et al.* (1994) in which the twist in the helicoidal architecture is directly imposed by the presence of other hemicelluloses mediating the helicity parameters without undergoing any significant reorientation. This imposes a constraint on the possibility of cell-wall expansion or contraction during growth, relevant to predictions of recent theories of cell-wall development (Haas *et al.*, 2020). Taken together, our results indicate that cellulosic



helical patterning is not formed by mechanical reorientation of the microfibrils driven by dehydration or compression, but rather represents a direct consequence of the way these fibrils are laid down, most likely directed by the chemical composition of the cell wall.

Our ongoing research on fruit development in *P. japonica* has hitherto concentrated on the use of this new technique to understand cell-wall structural changes during growth. However, our observations suggest several other avenues of research. Comparison of the fruits with those of *Pollia condensata* (Vignolini *et al.*, 2012) is instructive. Both species share optically reflective helicoidal cell walls, although – as we report here – in most of the cells of *P. japonica*, the internal cavity is filled with granular cell contents with many refractive index interfaces that are not observed in *P. condensata*. The transition to the final stage of maturation in *P. japonica*, when dehydration leaves granular cell contents inside the cell, is its strongest deviation from the appearance of *P. condensata*. This appears to explain the difference between the matte appearance of *P. japonica* and the pointillist appearance of *P. condensata* fruits. Further research on this material and optical effect and its visual adaptation would be valuable. Another extension to the work reported here would be in further analysis of the reflectance peak during development, for example in examining the intensity change in the later developmental stages, and further improvement of the model to make it predictive of layer number.

Here, we successfully employed an optical model to monitor at the nanoscale level the helicoidal architecture of the cell wall. Very little work exists on the development of structural colour so far, due to the difficulties in sampling and imaging the photonic structures accounting for these effects. Previous studies on the development of structural colour have focused on insects and on sampling of specimen averages (Onelli *et al.*, 2017) or electron microscopy of fixed dead material (Ghiradella, 1989). Our results show how standard optical spectroscopy of helicoidal architectures can be applied to living cells within a developing tissue and provide a quantitative insight into the mechanisms of interaction between developing biological materials at length scales 50 times smaller than the traditional resolution limit of optical microscopy, without the need for fluorescent tagging, staining or invasive and destructive sectioning. We anticipate that this technique will be applied to improve future understanding of other biological structurally coloured materials.








## Acknowledgements

This work was supported by the EPSRC NanoDTC EP/G037221/1 (RM), BBSRC David Phillips fellowship [BB/K014617/1], ERC SeSaME ERC-2014-STG H2020 639088 (SV), EU Marie Curie actions (Nanopetals to EM and BJG), and EPSRC NanoDTC EP/G037221/1 and EP/R513179/1 (RM). We thank Villads Johansen and Lisa Steiner for useful discussions. We are grateful to Matthew Dorling for care of plants. All of the research data supporting the publication are included in the publication, the supplementary material, and as raw data at <https://doi.org/10.17863/CAM.65896>. We declare we have no competing interests.

## Author contributions

RM, EM, BJG and SV conceptualized the study and the methodology; RM carried out optical measurement, modelling and formal analysis; EM, PJR, CJP and MC carried out SEM/TEM imaging; RM wrote the original draft; and all authors discussed, reviewed and edited the text to produce the final version.

## ORCID

Maria Conejero  <https://orcid.org/0000-0002-1138-7162>  
 Beverley J. Glover  <https://orcid.org/0000-0002-6393-819X>  
 Rox Middleton  <https://orcid.org/0000-0002-5309-3517>  
 Edwige Moyroud  <https://orcid.org/0000-0001-7908-3205>  
 Christina J. Prychid  <https://orcid.org/0000-0002-9165-8523>  
 Paula J. Rudall  <https://orcid.org/0000-0002-4816-1212>  
 Silvia Vignolini  <https://orcid.org/0000-0003-0664-1418>

## References

- Bartholemew B, Boufford DE, Chen QH, Fang SZ, Qi JG, Spongberg SA, Tsi ZH, Tu YL, Wang PS, Xiang YH *et al.* (1986). *Pollia japonica* Thunb. In: *Sino-American Guizhou botanical expedition no 155 (Ed.)*, plants of Guizhou, China. Leiden, the Netherlands: Naturalis Biodiversity Center – Botany Catalogues. [WWW document] URL [https://bioportal.naturalis.nl/multimedia/L.3756832\\_0834225730/term=Pollia&from=869?language=en&back#prettyPhoto](https://bioportal.naturalis.nl/multimedia/L.3756832_0834225730/term=Pollia&from=869?language=en&back#prettyPhoto) [accessed 9 March 2021].
- Belamie E, Mosser G, Gobeaux F, Giraud-Guille M-M. 2006. Possible transient liquid crystal phase during the laying out of connective tissues:  $\alpha$ -chitin and collagen as models. *Journal of Physics: Condensed Matter* **18**: S115–S129.
- Berremans DW. 1972. Optics in stratified and anisotropic media: 4x4-matrix formulation. *Journal of the Optical Society of America* **62**: 502–510.
- Bouligand Y. 1972. Twisted fibrous arrangements in biological materials and cholesteric mesophases. *Tissue & Cell* **4**: 189–217.
- Chen PY, Lin AYM, McKittrick J, Meyers MA. 2008. Structure and mechanical properties of crab exoskeletons. *Acta Biomaterialia* **4**: 587–596.
- Dumanli AG, Kamita G, Landman J, van der Kooij H, Glover BJ, Baumberg JJ, Steiner U, Vignolini S. 2014. Controlled, bio-inspired self-assembly of cellulose-based chiral reflectors. *Advanced Optical Materials* **2**: 646–650.
- Ghiradella HT. 1989. Structure and development of iridescent butterfly scales: lattices and laminae. *Journal of Morphology* **202**: 69–88.
- Giraud-Guille M-M. 1998. Plywood structures in nature. *Current Opinion in Solid State and Materials Science* **3**: 221–227.
- Haas KT, Wightman R, Meyerowitz EM, Peaucelle A. 2020. Pectin homogalacturonan nanofilament expansion drives morphogenesis in plant epidermal cells. *Science* **367**: 1003–1007.
- Jacobs M, Lopez-García M, Phrathep O, Lawson T, Oulton R, Whitney H (2016). Photonic crystal structure of *Begonia* chloroplasts enhances photosynthetic efficiency. *Nature Plants* **2**: 16162. doi: 10.1038/nplants.2016.162
- King MV. 1991. Dimensional changes in cells and tissues during specimen preparation for the electron microscope. *Cell Biophysics* **18**: 31–55.
- Kinoshita S, Yoshioka S. 2005. Structural colors in nature: the role of regularity and irregularity in the structure. *ChemPhysChem* **6**: 1442–1459.
- Mcdonald LT, Finlayson ED, Wilts BD, Vukusic P, Mcdonald LT. 2017. Circularly polarized reflection from the scarab beetle *Chalcothea smaragdina*: light scattering by a dual photonic structure. *Interface Focus* **7**: 20160129.
- Middleton R, Steiner U, Vignolini S. 2016. Bio-mimetic structural colour using biopolymers. In: Bruns N, Kilbinger AFM, eds. *Bio-inspired polymers*. Cambridge, UK: Royal Society of Chemistry, 561–591.
- Neville AC. 1985. Molecular and mechanical aspects of helicoid development in plant cell walls. *BioEssays* **3**: 4–8.

- Neville AC, Levy S. 1984. Helicoidal orientation of cellulose microfibrils in *Nitella opaca* internode cells: ultrastructure and computed theoretical effects of strain reorientation during wall growth. *Planta* **162**: 370–384.
- Onelli OD, Van De Kamp T, Skepper JN, Powell J, Rolo TDS, Baumbach T, Vignolini S, Rolo S, Baumbach T, Vignolini S. 2017. Development of structural colour in leaf beetles. *Scientific Reports* **7**: 1–9.
- Oseen CW. 1932. The theory of liquid crystals. *Transactions of the Faraday Society* **29**: 833–889.
- Parker AR, McKenzie DR, Large MCJ. 1998. Multilayer reflectors in animals using green and gold beetles as contrasting examples. *Journal of Experimental Biology* **201**: 1307–1313.
- Parker RM, Guidetti G, Williams CA, Zhao T, Narkevicius A, Vignolini S, Frka-Petesic B. 2017. The self-assembly of cellulose nanocrystals: hierarchical design of visual appearance. *Advanced Materials* **30**: e1704477.
- Reis D, Vian B, Chanzy H, Roland JC. 1991. Liquid crystal-type assembly of native cellulose-glucuronoxylans extracted from plant cell wall. *Biology of the Cell* **73**: 173–178.
- Reis D, Vian B, Roland JJ-C, Boon ME, Leyden P, Phytopathologie LD. 1994. Cellulose-glucuronoxylans and plant cell wall structure. *Micron* **25**: 171–187.
- Roland JC, Reis D, Vian B, Satiat-Jeuemaitre B, Mosiniak M. 1987. Morphogenesis of plant cell walls at the supramolecular level: internal geometry and versatility of helicoidal expression. *Protoplasma* **140**: 75–91.
- Sharma V, Crne M, Park JO, Srinivasarao M. 2009. Structural origin of circularly polarized iridescence in jeweled beetles. *Science* **325**: 449–451.
- Steiner LM, Ogawa Y, Johansen VE, Lundquist C, Whitney H, Vignolini S. 2018. Structural colours in the frond of *Microsorium thailandicum*. *Interface Focus* **9**: 20180055.
- Strout G, Russell SD, Pulsifer DP, Erten S, Lakhtakia A, Lee DW. 2013. Silica nanoparticles aid in structural leaf coloration in the Malaysian tropical rainforest understorey herb *Mapania caudata*. *Annals of Botany* **112**: 1141–1148.
- Sykes D, Hartwell R, Bradley RS, Burnett TL, Hornberger B, Garwood RJ, Withers PJ. 2019. Time-lapse three-dimensional imaging of crack propagation in beetle cuticle. *Acta Biomaterialia* **86**: 109–116.
- Vignolini S, Gregory T, Kolle M, Lethbridge A, Moyroud E, Steiner U, Glover BJ, Vukusic P, Rudall PJ. 2016. Structural colour from helicoidal cell-wall architecture in fruits of *Margaritaria nobilis*. *Journal of the Royal Society Interface* **13**: 20160645.
- Vignolini S, Rudall PJ, Rowland AV, Reed A, Moyroud E, Faden RB, Baumberg JJ, Glover BJ, Steiner U. 2012. Pointillist structural color in *Pollia* fruit. *Proceedings of the National Academy of Sciences, USA* **109**: 15712–15715.

## Supporting Information

Additional Supporting Information may be found online in the Supporting Information section at the end of the article.

**Fig. S1** Full dataset for one cell and the use of a pigment-only cell control dataset to extract the purely structural colour peak.

**Fig. S2** Full dataset for the spectral series from one cell shown simplified in Fig. 1(j).

**Fig. S3** Map of the first set of measured cells in parallel and cross-polarization.

**Fig. S4** Electron micrographs showing higher magnification SEMs and TEMs for cells at every maturation stage.

**Fig. S5** Individual fits and residuals for each cell's peak reflectance wavelength for both cell sets.

Please note: Wiley Blackwell are not responsible for the content or functionality of any Supporting Information supplied by the authors. Any queries (other than missing material) should be directed to the *New Phytologist* Central Office.